



# EurJIC

European Journal of Inorganic Chemistry

 **Chemistry  
Europe**  
European Chemical  
Societies Publishing

## Accepted Article

**Title:** Template-assisted regio-selective identification of metal ions on coumarin-furan conjugated chemosensors; AIEE effect and photo-switching pH indicator by ICT

**Authors:** Ashish Kumar, Sumit Kumar Hira, and Swapan Dey

This manuscript has been accepted after peer review and appears as an Accepted Article online prior to editing, proofing, and formal publication of the final Version of Record (VoR). This work is currently citable by using the Digital Object Identifier (DOI) given below. The VoR will be published online in Early View as soon as possible and may be different to this Accepted Article as a result of editing. Readers should obtain the VoR from the journal website shown below when it is published to ensure accuracy of information. The authors are responsible for the content of this Accepted Article.

**To be cited as:** *Eur. J. Inorg. Chem.* 10.1002/ejic.202000583

**Link to VoR:** <https://doi.org/10.1002/ejic.202000583>

WILEY-VCH

# Template-assisted regio-selective identification of metal ions on coumarin-furan conjugated chemosensors; AIEE effect and photo-switching pH indicator by ICT

Ashish Kumar,<sup>[a]</sup> Sumit Kumar Hira,<sup>[b]</sup> and Swapan Dey\*<sup>[a]</sup>

[a] Dr. Ashish Kumar and Dr. Swapan Dey  
Department of Chemistry,  
Indian Institute of Technology (ISM), Dhanbad  
Dhanbad, Jharkhand-826004, India.  
E-mail: swapan@iitism.ac.in; Fax: +91 326 2296563; Tel: +91 326 2235607.  
\* Presently working as a Research Associate in the Department of Chemistry  
University of Delhi, Delhi, India

[b] Dr. Sumit Kumar Hira  
Department of Zoology  
University of Burdwan, Burdwan  
Burdwan, West Bengal 713104, India

Supporting information for this article is given via a link at the end of the document.

**Abstract:** A coumarin-furan conjugated Schiff base chemosensor (**R1**) of straightforward design showed an excellent aggregation-induced emission enhancement effect in ACN-H<sub>2</sub>O mixtures of different ratios, which was confirmed by *field emission scanning electron microscopy* (FESEM) and supported by *Dynamic Light Scattering* (DLS). **R1** identified three metal ions (Pb<sup>2+</sup>, Hg<sup>2+</sup> and Cu<sup>2+</sup>) in colorimetric and fluorometric techniques with an *intramolecular charge transfer* (ICT) off-on mechanism. The space specificity of the metal ions (Hg<sup>2+</sup> and Cu<sup>2+</sup>) resulted in hydrolysis of -CH=N- functionality of the sensor. The latter also exhibited excellent sensitivity in acidic conditions by blocking ICT and remained stable in neutral to basic pH. Cell viability and microscopic fluorescence experiments revealed that **R1** is cytocompatible and may be used for the detection of Pb<sup>2+</sup>, Hg<sup>2+</sup>, and Cu<sup>2+</sup> ions in living cells.

## Introduction

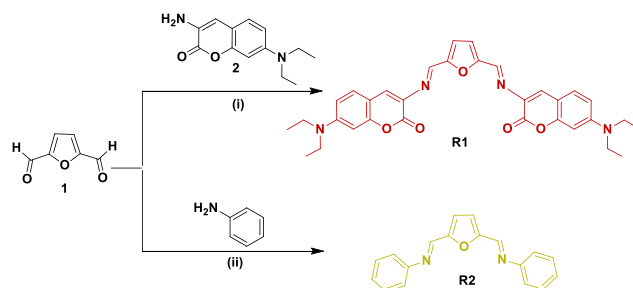
Aggregation-induced emission enhancement (AIEE) is one of the hottest topics in current research, and it has been broadly studied because of the promising applications in organic, supramolecular, medicinal, and material chemistry.<sup>1</sup> The AIEE based molecules are used in real-time applications such as organic light-emitting diodes,<sup>2,3</sup> chemosensors,<sup>4-6</sup> fluorescent bio-probes,<sup>7-9</sup> heavy and noxious metal ions sensors,<sup>10-12</sup> catalysts, organic molecular transformations<sup>13</sup>, etc. In 2001, Tang's group first discovered the innovative phenomenon of aggregation-induced emission (AIE), which attracted much attention and solved many critical problems.<sup>14-16</sup> They developed and selected the molecules having tetraphenylethylene (TPE)<sup>17-19</sup> and hexaphenylsilole (HPS)<sup>20</sup>, moieties which showed good AIE or AIEE effect. In addition to this, other molecules having pyrans,<sup>21</sup> butadienes,<sup>22</sup> and fulvenes<sup>23</sup> were also there to explain aggregation better. Small fluorescent probes have several advantages in the field of sensing as they can sense ions and neutral molecules with a low limit of detection, fast response toward selective analytes and high quantum yield etc.<sup>10,24</sup> Coumarin is one of these, possessing highly fluorescent properties and working as a good sensor.<sup>25,26</sup>

Mercury and Lead are highly toxic heavy metal ions and have been widespread in water, soil and air by numerous human activities such as gold production, coal plants etc.<sup>10</sup> The shallow levels of Hg<sup>2+</sup> and Pb<sup>2+</sup> can create various illnesses like impairments, anemia, neurological damage, memory loss, nerve disorders, reduced IQ etc.<sup>27,28</sup> Copper is an essential element in the human body which performs a significant role in various physiological processes and biological functions.<sup>29,30</sup>

## Results and Discussion

A sensor is presented with a region-selective molecular cavity (**R1**) for three specific metal ions (Cu<sup>2+</sup>, Hg<sup>2+</sup>, and Pb<sup>2+</sup>) by fluorometric and colorimetric assays with a low limit of detections (0.14 × 10<sup>-6</sup> M, 0.032 × 10<sup>-6</sup> M and 41 × 10<sup>-6</sup> M, respectively) (SI; Figure S23-S25) and complexation occurred with Cu<sup>2+</sup>, Hg<sup>2+</sup> and Pb<sup>2+</sup> in 1:1, 1:1 and 2:1 stoichiometric, respectively with high quantum yield (**Table 1**). In addition to that, it also exhibited strong AIEE in a mixture of acetonitrile-water (ACN-H<sub>2</sub>O). A truncated sensor **R2** has also been reported, which has three binding sites to encapsulate the metal ions.

**Scheme 1.** Synthesis of **R1** and **R2**.



**Reagent and conditions:** (i) Ethanol, acetic acid, reflux, 24 h; (ii) Ethanol, reflux, 24h.

Herein, a new Schiff base chemosensor **R1** has been synthesized by the simple condensation reaction of two equivalents of 3-amino-7-(diethylamino)-2H-chromen-2-one (**2**) with furan 2,5-dicarboxylaldehyde (**1**). On the other side, **R2** has been made by the reaction between two equivalents of aniline and furan 2,5-dicarboxylaldehyde in a similar fashion (**Scheme 1**). Both the chemosensors were successfully obtained in good yield and well-characterized by  $^1\text{H-NMR}$ ,  $^{13}\text{C-NMR}$ , LC-MS, and FT-IR. Photophysical studies were carried out in UV-visible and fluorescence spectrophotometer. The morphological changes of AIEE properties and the complex of metal ions were recorded by FESEM. **R2** was reported as a supportive chemosensor for the better and exact explanation of multi-point complexation of **R1** with metal ions like  $\text{Pb}^{2+}$ ,  $\text{Hg}^{2+}$ , and  $\text{Cu}^{2+}$ . Chemosensors **R1** and **R2** have an almost common binding site, however, only **R2** responded on  $\text{Cu}^{2+}$  and  $\text{Hg}^{2+}$  ions.

### Photophysical studies

The visible and fluorescence colour changes of **R1** ( $c = 1.8 \times 10^{-6}$  M in ACN at  $\text{pH} = 7.0 \pm 0.05$ , HEPES buffer) was investigated with different metal ions ( $\text{Al}^{3+}$ ,  $\text{Cr}^{3+}$ ,  $\text{Mn}^{2+}$ ,  $\text{Fe}^{3+}$ ,  $\text{Pb}^{2+}$ ,  $\text{Hg}^{2+}$ ,  $\text{Cu}^{2+}$ ,  $\text{Co}^{2+}$ ,  $\text{Ni}^{2+}$ ,  $\text{Zn}^{2+}$ ,  $\text{Cd}^{2+}$ ,  $\text{Ag}^+$ ,  $c = 2.5 \times 10^{-4}$  M) in UV-grade acetonitrile. The orange colour solution of **R1** became deep blue, golden and light orange, respectively adding  $\text{Pb}^{2+}$ ,  $\text{Hg}^{2+}$ , and  $\text{Cu}^{2+}$  ions. Under long wavelength (365 nm) UV light, non-fluorescent **R1** exhibited fluorescence emission on treating with  $\text{Hg}^{2+}$  and  $\text{Cu}^{2+}$  ions. So, **R1** showed colorimetric selectivity for  $\text{Pb}^{2+}$ ,  $\text{Hg}^{2+}$  and  $\text{Cu}^{2+}$  and fluorometric sensitivity for  $\text{Hg}^{2+}$  and  $\text{Cu}^{2+}$  ions (**Fig. 1a** and **1b**).



**Figure 1.** Naked eye detection of different metal ions ( $c = 2.5 \times 10^{-4}$  M) by **R1** ( $c = 1.8 \times 10^{-6}$  M in ACN at  $\text{pH} = 7.0 \pm 0.05$ , HEPES buffer) (a) Visible colour change (b) fluorescence change were taken under long wavelength (365 nm) hand-held UV-light.

UV-visible titration of **R1** ( $c = 1.8 \times 10^{-6}$  M in ACN at  $\text{pH} = 7.0 \pm 0.05$ , HEPES buffer) has been carried out with the same metal ions ( $c = 2.5 \times 10^{-4}$  M) in freshly prepared stock solution. **R1** exhibited absorption maxima at  $\lambda_{\text{max}}$  486 nm. However, the peak intensity and maxima were accordingly changed on the regular addition of  $\text{Cu}^{2+}$ ,  $\text{Hg}^{2+}$ , and  $\text{Pb}^{2+}$ . The addition of  $\text{Cu}^{2+}$  decreased the peak intensity at 486 nm and also seemed to induce a hypsochromic from 486 nm to 423 nm (**Fig. 2a**). The absorbance of **R1** itself at 486 nm was getting reduced, and a new peak at  $\lambda_{\text{max}}$  605 nm appeared with increasing  $\text{Hg}^{2+}$  ion concentration. This happens only upon complexation between **R1** and  $\text{Hg}^{2+}$ . After some time, that peak at  $\lambda_{\text{max}}$  605 nm was also disappeared and two new peaks at  $\lambda_{\text{max}}$  325 nm and 462 nm were developed, which indicated the imine bond hydrolysis and the compound **2** and **3** [(E)-5-((7-(diethylamino)-2-oxo-2H-

chromen-3-yl)imino)methyl)furan-2-carbaldehyde] were reproduced (**Scheme 2**). On the other hand, in the presence of  $\text{Pb}^{2+}$  ion, the absorption of **R1** ( $\lambda_{\text{max}}$  486 nm) declined continuously, and a new broad peak at  $\lambda_{\text{max}}$  572 nm was found. With the continuous addition of  $\text{Pb}^{2+}$ , the complex solution became saturated, and one isosbestic point was observed at 550 nm (**Fig. 2c**). The DLS analysis of complexes **R1** with  $\text{Cu}^{2+}$ ,  $\text{Hg}^{2+}$ , and  $\text{Pb}^{2+}$  were studied, which showed that the complex **R1**: $\text{Cu}^{2+}$  and **R1**: $\text{Hg}^{2+}$  gives two different sizes, but only one dimension of molecules in the solution was found in the complex **R1**: $\text{Pb}^{2+}$  (SI, Figure S26-S28).

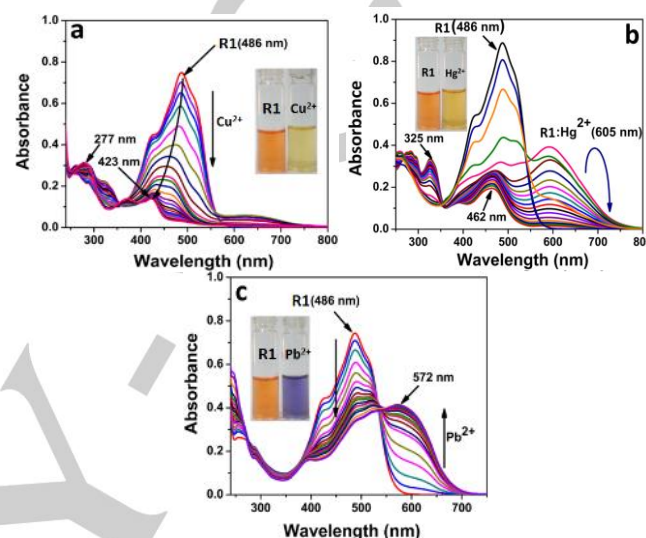


**Figure 2.** UV-visible titration spectra of **R1** ( $c = 1.8 \times 10^{-6}$  M in ACN at  $\text{pH} = 7.0 \pm 0.05$ , HEPES buffer) with (a)  $\text{Cu}^{2+}$ , (b)  $\text{Hg}^{2+}$  and (c)  $\text{Pb}^{2+}$  (ions concentration  $2.5 \times 10^{-4}$  M).

The fluorescence titration studies of **R1** were carried out with  $\text{Cu}^{2+}$  and  $\text{Hg}^{2+}$ , but not with  $\text{Pb}^{2+}$  as the earlier did not show any fluorescence behavior (**Fig. 1b**). **Fig. 3a** and **3b** represent the fluorescence titration spectra where the fluorescence emission intensity of **R1** increased sharply on the addition of one equivalent  $\text{Cu}^{2+}$  and  $\text{Hg}^{2+}$ . A new peak was generated at  $\lambda_{\text{em}}$  497 nm with a 5.0 fold intensity enhancement with  $\text{Hg}^{2+}$  compare to  $\text{Cu}^{2+}$ .

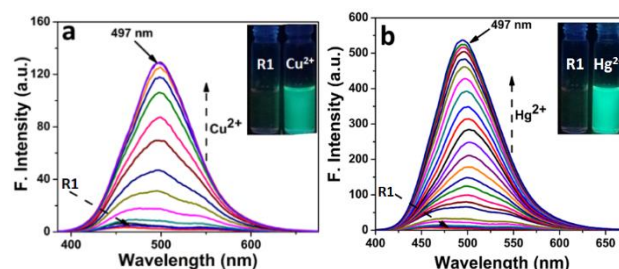


**Figure 3.** Fluorescent titration spectra of **R1** ( $c = 1.8 \times 10^{-6}$  M in ACN at  $\text{pH} = 7.0 \pm 0.05$ , HEPES buffer,  $\lambda_{\text{ex}} = 365$  nm) with (a)  $\text{Cu}^{2+}$  and (b)  $\text{Hg}^{2+}$  ( $c = 2.5 \times 10^{-4}$  M); insets: visible colour changes under 365 nm UV light irradiation.

A simple conjugation was found in **R2** so that the photophysical properties may be changed upon disturbing conjugation. It has been prepared as an analog of **R1** as they have almost the

same binding sites. The UV-visible titration of **R2** has also been carried out with different metal ions, and it was found that **R2** was sensitive towards  $\text{Cu}^{2+}$  and  $\text{Hg}^{2+}$  only, but not to  $\text{Pb}^{2+}$  (Fig. 4). So this observation proved that both the coumarin moieties of **R1** were directly involved in binding of  $\text{Pb}^{2+}$  ion (Scheme 2).

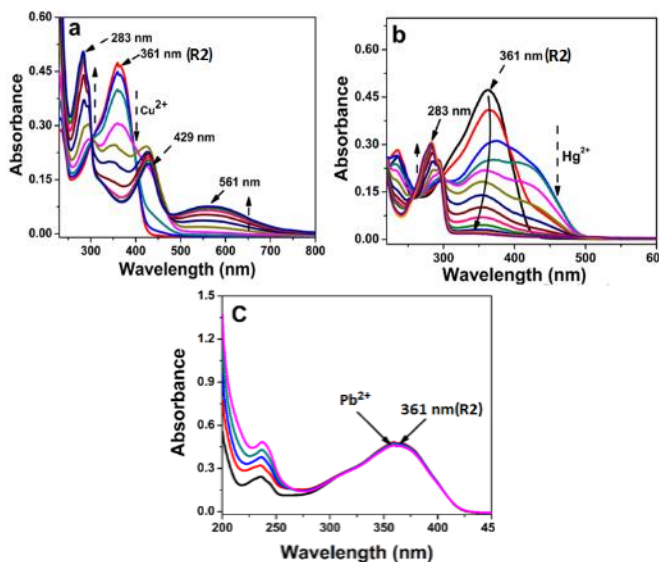


**Figure 4.** UV-visible titration spectra of **R2** ( $c = 1.8 \times 10^{-6}$  M in ACN at pH =  $7.0 \pm 0.05$ , HEPES buffer) with (a)  $\text{Cu}^{2+}$ , (b)  $\text{Hg}^{2+}$  and (c)  $\text{Pb}^{2+}$  ( $c = 2.5 \times 10^{-4}$  M).

### Aggregation-Induced Emission effect

**R1** was initially non-fluorescent, and the fluorescence intensity in ACN was almost a flat line corresponding to the abscissa. When the fraction of  $\text{H}_2\text{O}$  was increased continuously, the fluorescence of **R1** was turned on, and the emission intensity enhanced up to 70%  $\text{H}_2\text{O}$  content in ACN. In the presence of  $\text{H}_2\text{O}$ , isomerization of free rotation of imine double bond (C=N) of coumarin at 3 position was restricted by the aggregation and, accordingly, the transfer of electrons of diethylamine was blocked,<sup>31</sup> which caused the enhancement of fluorescence. This change was recorded with the spectrophotometer as well as through the naked eye under a long wavelength UV light (Fig. 5b).

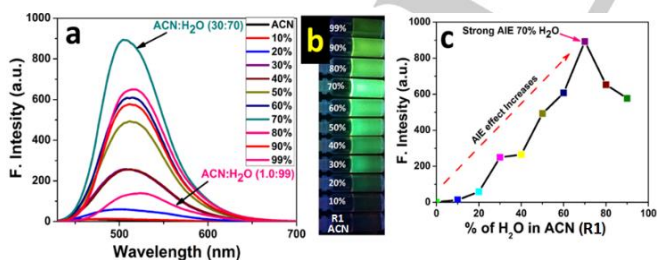


**Figure 5.** AIEE studies of **R1** ( $c = 1.8 \times 10^{-6}$  M) in different ACN- $\text{H}_2\text{O}$  mixed solvents ( $\lambda_{\text{ex}} = 365$  nm); (a) fluorescence spectra (b) naked eye observation under long-wavelength 365 nm UV light (c) change in fluorescence intensity in different ratio of  $\text{H}_2\text{O}$ -ACN.

The morphology of the sensor and the complex in aggregation were recorded using FESEM (Fig. 6) and DLS analysis (Fig. 7). All the composite images of FESEM were taken in the solid-state. The samples were prepared by the drop cast method on a

glass slide, and it was dried at  $60^\circ\text{C}$  for 5.0 hrs under the oven. A needle-shaped texture of **R1** was observed in pure ACN solvent (Fig. 6a). The fluorescence intensity was recorded at a maximum when the  $\text{H}_2\text{O}$  content reached 70 % in ACN. In this condition, the needle texture of **R1** disappeared and aggregation was found (Fig. 6b). The study was continued for the complexes of **R1** with metal ions ( $\text{Cu}^{2+}$ ,  $\text{Hg}^{2+}$ , and  $\text{Pb}^{2+}$ ). Fig. 6c and Fig. 6d represented almost the same morphology, a sheet-like texture upon addition of  $\text{Cu}^{2+}$  and  $\text{Hg}^{2+}$ . However, the addition of  $\text{Pb}^{2+}$  produced a spherical morphology and it was totally different as compared to the complexes **R1**: $\text{Cu}^{2+}$  and **R1**: $\text{Hg}^{2+}$  (Fig. 6f).

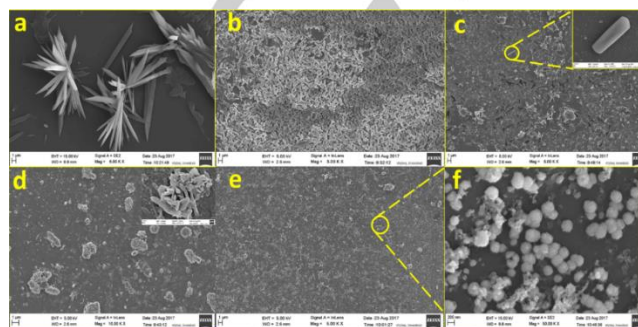


**Figure 6.** FESEM images of **R1** and its complexes (a) Only **R1** in ACN (b) only **R1** in 70%  $\text{H}_2\text{O}$  in ACN (c) complex **R1**: $\text{Cu}^{2+}$  (d) complex **R1**: $\text{Hg}^{2+}$  (e) complex **R1**: $\text{Pb}^{2+}$  (f) high resolution of **R1**: $\text{Pb}^{2+}$ .

In previous reports, it was found that the change in fluorescence properties occurred due to aggregation or disaggregation of the sensors.<sup>15</sup> For a better explanation, DLS analysis was carried out and found 2.2 nm size of **R1** existed in pure ACN. Upon addition of  $\text{H}_2\text{O}$  to ACN, the size of **R1** was continuously increasing and it became maximum upto 157.4 nm ( $\text{H}_2\text{O}$ -ACN, 70-30%). The highest fluorescence intensity has been achieved due to the maximum aggregation. The emission intensity was further decreased on increasing  $f_w$ , which may be happened due to interference of size of aggregated molecules (Fig. 7).<sup>32</sup>

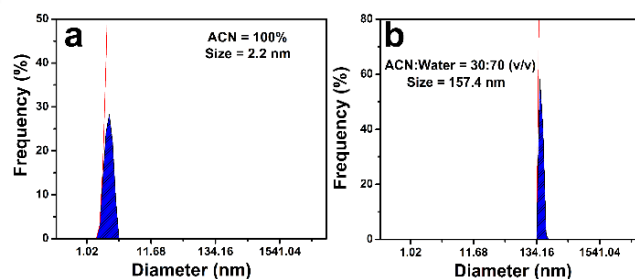


**Figure 7.** DLS analysis of **R1** ( $c = 1.8 \times 10^{-6}$  M) in (a) ACN (b) 70%  $\text{H}_2\text{O}$  in ACN.

### Performance of **R1** in different pH ranges

The effect of pH on **R1** was studied at various pH (1.0 to 13) using UV-visible and fluorescence spectroscopic techniques (Fig. 8). No change in absorption ( $\lambda_{\text{max}} 486$  nm) occurred from neutral to basic pH (7.0 to 13.0 pH). The peak absorbance decreased with decreasing pH (from 7.0 to 1.0 pH), and it was nearly insignificant at highly acidic (pH 1.0) conditions. The orange colour of **R1** turned to yellow and then nearly colorless on decreasing pH (Fig. 8a). The change in fluorescence

intensity was also investigated in the same manner and it was found that **R1** was non-fluorescent at neutral to basic pH (7.0 to 13) and the fluorescence intensity increased continuously from neutral to pH 1.0 and consequently one new emission peak at  $\lambda_{\max}$  497 nm appeared. The change in fluorescence intensity was also observed through the naked eye after irradiation with a long-range UV light, looking like a strong aqua blue fluorescence. The difference in fluorescence properties was due to trapping of lone pair of the ethylamine nitrogen by a proton and prohibited ICT.<sup>33</sup>

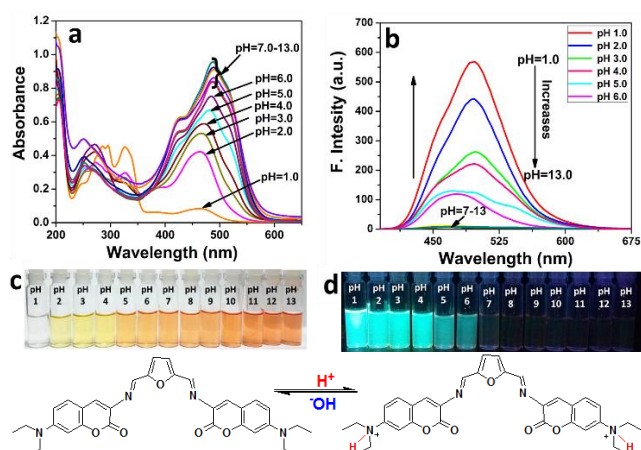


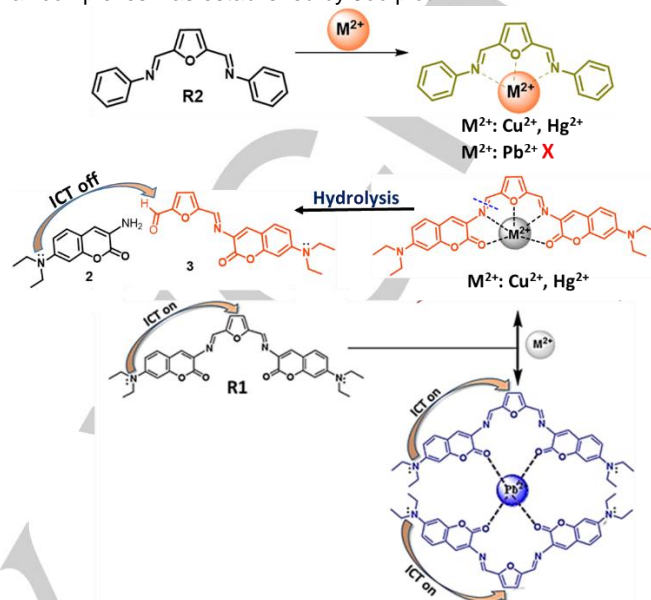
**Figure 8.** Effect of pH (1.0 to 13.0) on chemosensor **R1** ( $c = 1.8 \times 10^{-6}$  M in ACN at pH =  $7.0 \pm 0.05$ , HEPES buffer) (a) UV-visible spectra (b) fluorescence spectra (c) visible colour changes and (d) colour change under UV-lamp of 365 nm; and its protonation-deprotonation mechanism.

### Possible mode of binding

**R1** recognized three metal ions ( $\text{Cu}^{2+}$ ,  $\text{Hg}^{2+}$  and  $\text{Pb}^{2+}$ ) separately with different photophysical properties. When **R1** was bonded to  $\text{Cu}^{2+}$  and  $\text{Hg}^{2+}$ , the orange colour of **R1** was rehabilitated into golden and light yellow, respectively and the property has been changed to exhibit strong fluorescence, accordingly (Fig. 3). However, the orange colour **R1** was turned to deep blue instantly on the addition of  $\text{Pb}^{2+}$  (Fig. 1). However, chemosensor **R2** recognized  $\text{Cu}^{2+}$  and  $\text{Hg}^{2+}$ , not  $\text{Pb}^{2+}$ . This was due to the optimum cavity size created by two imine N-atoms and one O-atom of the furan ring, where both  $\text{Cu}^{2+}$  and  $\text{Hg}^{2+}$  could easily be encapsulated. The size of  $\text{Pb}^{2+}$  is significantly larger than other mentioned metal ions (ionic radius  $\text{Cu}^{2+}$ ,  $\text{Hg}^{2+}$  and  $\text{Pb}^{2+}$  are 73 pm, 102 pm, and 119 pm, respectively)<sup>34</sup> and it was incorporated in the template created by two lactone O-atoms of the coumarin moiety. According to UV-vis titration of **R1** and **R2**, the result suggested that the chemosensor **R1** strongly binds  $\text{Cu}^{2+}$  and  $\text{Hg}^{2+}$  into its cavity, constructed by the two imine N-atoms and one O-atom of the furan ring. As a result, a bathochromic shifting of wavelength from 486 nm, which indicated the metal ion interacted with the O-atom of coumarin carbonyls.<sup>35</sup> But, after few seconds, the shifted peak was shrunk due to the breaking of bond.

The possible photophysical changes were recorded on the basis of the binding mode of metal ions and happened through ICT (scheme 2). When  $\text{Cu}^{2+}$  and  $\text{Hg}^{2+}$  bind, the imine bond of **R1** became hydrolyzed to produce compound **2** and **3** (Scheme 2). This was confirmed by  $^1\text{H-NMR}$  and mass spectroscopy. Upon hydrolysis, the peak of imine hydrogen at  $\delta$  9.49 ppm almost vanished and two new peaks were generated at  $\delta$  9.79 ppm and

$\delta$  9.66 ppm for aldehyde (CHO) and imine ( $-\text{C}=\text{N}-$ ) functionality, respectively.<sup>36</sup> The same result was not found on employing  $\text{Pb}^{2+}$  to **R1**. In mass spectra, two peaks were found at  $m/z$  233 (compound **2**+H) and 339 (compound **3**+H) on the treatment of either  $\text{Cu}^{2+}$  or  $\text{Hg}^{2+}$  to **R1**. However, the binding stoichiometry of all complexes was established by Job plot.



**Scheme 2.** The possible mode of binding of  $\text{Cu}^{2+}$ ,  $\text{Hg}^{2+}$  and  $\text{Pb}^{2+}$  with **R1** and **R2**.

### Quantum Yield (Q)

The quantum yield for different conditions was calculated and summarised in Table 1 by applying the standard formula (SI, Page 14).<sup>37</sup>

**Table 1.** Quantum yield of **R1** with different conditions

Quantum yield (Q)					
		Aggregation		Complexation	
pH	Q	H <sub>2</sub> O %	Q	R1 with	Q
7.0	0.001	10	0.001	$\text{Cu}^{2+}$	0.06
6.0	0.05	20	0.002	$\text{Hg}^{2+}$	0.19
5.0	0.07	30	0.01		
4.0	0.16	40	0.05		
3.0	0.24	50	0.14		
2.0	0.27	60	0.21		
1.0	0.33	70	0.29		
		80	0.22		
		90	0.18		

### Bio-imaging studies

The potential of furan-coumarin conjugated Schiff's base chemosensor (**R1**) for region-selective detection of  $\text{Pb}^{2+}$ ,  $\text{Hg}^{2+}$  and  $\text{Cu}^{2+}$  ions in living cells was investigated. The MTT assay for MCF-7 (breast adenocarcinoma) cells was used to determine the cytocompatibility of **R1**. In Fig. 9, the cell viability was greater than 80%, following treatment with the compound for 48 h. This result indicated that **R1** was safe and induced low cytotoxicity even at higher concentration (100  $\mu\text{M}$ ).

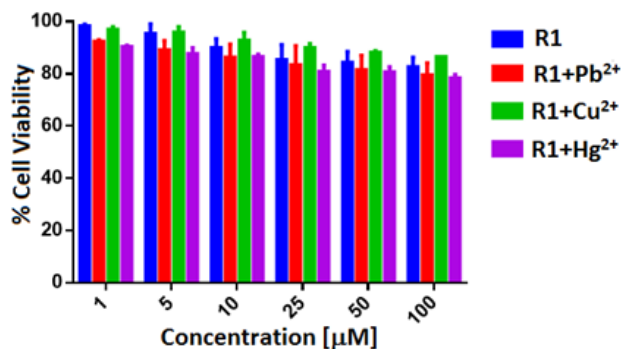


**Figure 9.** MTT assay of MCF-7 cells treated in the presence of **R1** (0–100 μM) incubated at 37°C for 48 hrs in the presence or absence of Cu<sup>2+</sup>, Hg<sup>2+</sup> and Pb<sup>2+</sup> metal ions.

Fluorescence imaging analysis was performed for demonstrating the bio-distribution of the compound in living cells using a Leica DMI600 fluorescent microscope. MCF-7 cells incubated with **R1** only did not produce any detectable fluorescence (**Fig. 10A-C**). However, after treatment with Hg<sup>2+</sup>, a bright green fluorescence was observed in the MCF-7 cells (**Fig. 10 J-L**). Overlaying of fluorescence and bright-field images showed that the fluorescence signals were localized in the intracellular areas, indicating the subcellular distribution of Hg<sup>2+</sup>, besides effective cell-membrane permeability for **R1**. The specificity of **R1** towards Hg<sup>2+</sup> ions was demonstrated by performing similar experiments using Cu<sup>2+</sup> and Pb<sup>2+</sup> ions in the absence of Hg<sup>2+</sup> ions. Cells were exposed to various concentrations (from 0 to 100 μM) of Cu<sup>2+</sup> or Pb<sup>2+</sup> ions in PBS and images were obtained using a Leica DMI600 fluorescent microscope after the addition of **R1**. In contrast to Hg<sup>2+</sup>, a competing metal ion like Cu<sup>2+</sup> displayed weak fluorescence at higher concentrations (100 μM tested) (**Fig. 10 G-I**). In the case of Pb<sup>2+</sup>, no fluorescence was observed at all.

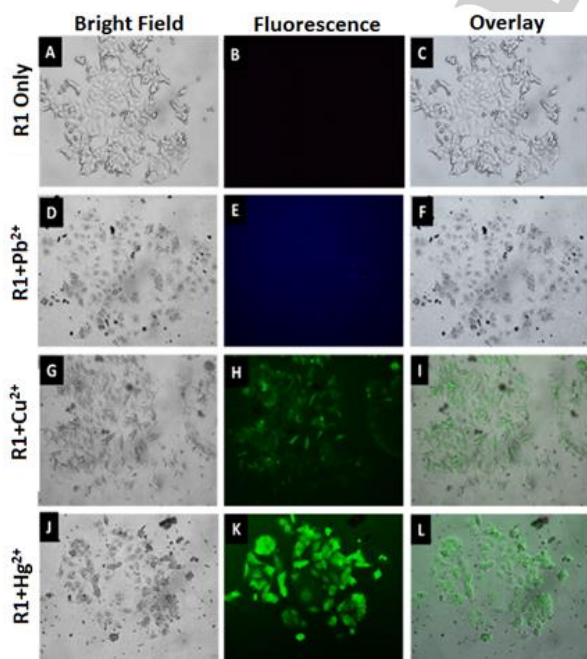


**Figure 10.** Fluorescence images of MCF-7 cells treated with **R1** and Pb<sup>2+</sup>, Cu<sup>2+</sup> and Hg<sup>2+</sup>. Bright-field image; fluorescence image and overlay image.

## Conclusion

In conclusion, the first template-assisted regio-selective coumarin-furan conjugated Schiff base chemosensor (**R1**) has been reported for the discrimination of highly toxic Hg<sup>2+</sup> and Pb<sup>2+</sup> ions in a straight forward manner. Moreover, **R1** selectively recognized three metal ions (Pb<sup>2+</sup>, Hg<sup>2+</sup>, and Cu<sup>2+</sup>) by colorimetric and fluorometric technique with an ICT *on-off* mechanism. It may also be used as a pH sensor and showed intense blue fluorescence in acidic condition due to protonation of lone pair of diethylamine, which blocked ICT. One analogous chemosensor, **R2** was also reported herewith for a better explanation of the mode of complexation. **R1** showed excellent AIEE in a different fraction of ACN-H<sub>2</sub>O. In the FESEM image, **R1** looked like aggregated morphology in ACN-H<sub>2</sub>O (30:70, v/v) and exhibited maximum aggregation. This has surprisingly enhanced fluorescence intensity by 180 fold and could observe without any difficulty through the naked eye. DLS analysis also confirmed the aggregation. The sensor was cyto-compatible and detected Pb<sup>2+</sup>, Hg<sup>2+</sup> and Cu<sup>2+</sup> ions in living cells.

## Experimental Section

### Materials and equipment used

All the chemicals and analytical grade solvents were obtained commercially from Merck and Sigma-Aldrich and used without purification. Metal perchlorates salts were prepared in the laboratory from the respective carbonate and nitrate salts. <sup>1</sup>H-NMR and <sup>13</sup>C-NMR spectra were recorded with a Bruker 400 MHz and 500 MHz spectrometers using CDCl<sub>3</sub> solvent. Mass spectra were analyzed by ESI source. UV-visible and fluorescence spectra were recorded with a PerkinElmer Lambda 365 and LS 55 instrument, respectively, using 10 mm path length of the cuvette. FT-IR spectra were recorded in the range of 4000 to 400 cm<sup>-1</sup> using KBr pellets.

### Synthesis of 1 and 2.

Compound **1**<sup>24</sup> and **2**<sup>16</sup> were synthesized according to the earlier reported methods.

### Synthesis of chemosensor R1

Furan 2,5-dicarbaldehyde (50 mg, 0.40 mmol) was completely dissolved in ethanol (20.0 mL) and 3-amino-7-diethylamino coumarin (200 mg, 0.86 mmol) was added, followed by a catalytic amount (4-5 drops) of acetic acid. The reaction mixture was stirred to complete after 24 h at reflux. Then the volume of the solvent was reduced. Finally, a red solid precipitate was obtained by further filtration washing with ethanol (30.0 mL). (75.0 mg, yield: 40.0 %). Melting point: 230°C.

**FT-IR (KBr, cm<sup>-1</sup>):** 3412 (H<sub>2</sub>O), 3141 (=C-H, str.), 2967 (-C-H, str.), 2924 (-C-H, str.), 1704 (C=O, str.), 1617 (C=N, str.), 1515 (C=C, str.).

**<sup>1</sup>H-NMR (400 MHz, CDCl<sub>3</sub>) of R1:** δ 9.49 (s, 2H), 7.839 (s, 2H), 7.34 (d, *J* = 8.8 Hz, 2H), 7.04 (s, 2H), 6.61 (d, *J* = 8.8 Hz, 2H), 6.50 (s, 2H), 3.42 (q, *J* = 7.2 Hz, 8H), 1.21 (t, *J* = 7.2 Hz, 12H).

**<sup>13</sup>C NMR (125 MHz, CDCl<sub>3</sub>) of R1:** δ 158.83, 155.14, 155.03, 150.79, 147.92, 139.62, 129.45, 126.82, 116.93, 109.45, 109.25, 96.98, 44.93, 12.50.

**ESI-MS (+) of R1:** Calculated  $C_{32}H_{33}N_4O_5$ : 553.2451 [M+H]; found: 553.2455 [M+H].

### Synthesis of R2

Furan 2,5-carbaldehyde (50 mg, 0.40 mmol) and aniline (100  $\mu$ L, excess) were dissolved in ethanol (20 mL) and refluxed for 12 h at 80°C. After completion of the reaction, the solvent was reduced and filtered. A yellow solid product was then washed with ethanol several times (20 mL) to get the pure product (yield: 80 %, 100.0 mg). Melting point: 138°C.

**FT-IR (KBr,  $cm^{-1}$ ):** 3401 (H<sub>2</sub>O), 3130 (=C-H, str.), 3074 (-C-H, str.), 1617 (C=N, str.), 1515 (C=C, str.).

**<sup>1</sup>H-NMR (400 MHz, CDCl<sub>3</sub>) of R2:**  $\delta$  8.41 (s, 2H), 7.41-7.378 (m, 6H), 7.26-7.25 (m, 4H) 7.15 (s, 2H).

**<sup>13</sup>C NMR (125 MHz, CDCl<sub>3</sub>) of R2:**  $\delta$  154.32, 151.05, 147.79, 129.31, 126.82, 121.10, 116.31

### Cell culture

MCF7 (ATCC® HTB-22™) cells were grown in RPMI-1640 supplemented with 10% FBS at 37°C and 5% CO<sub>2</sub>. Cells were plated in a 48 or 96 well culture plate and allowed to adhere for 24 h before experimentation.<sup>38</sup>

### Cell viability assay

The methyl thiazolyltetrazolium (MTT) assay was used to measure the cytotoxicity of R1 in MCF-7 cells.<sup>39</sup> MCF-7 cells were seeded in a 96-well cell culture plate. Various concentrations (0-100  $\mu$ M) of R1 were added to the cells. The cells were incubated at 37 °C under 5% CO<sub>2</sub> for 48 h. 10  $\mu$ L MTT (5 mg mL<sup>-1</sup>) was added to each well and incubated at 37°C under 5% CO<sub>2</sub> for 4 h. The MTT solution was removed and yellow precipitates (formazan) observed in plates were dissolved in 200  $\mu$ L of acidic isopropanol. Multiskan™ GO Microplate Spectrophotometer was used to measure the absorbance at 570 nm for each well. The viability of cells was calculated according to the following equation:

$$\% \text{ Cell Viability} = \left[ \frac{\text{Experimental OD}_{570}}{\text{Control OD}_{570}} \right] \times 100$$

### Fluorescence imaging

First, stock solutions of R1 were prepared in H<sub>2</sub>O/ACN solution. MCF-7 Cells were plated in a 48 well cell culture plate and allowed to adhere for 48 h. Experiment to assess the Hg<sup>2+</sup> uptake was performed in phosphate-buffered saline (PBS) in the presence of Hg(ClO<sub>4</sub>)<sub>2</sub>. The cells were treated with 25  $\mu$ M Hg(ClO<sub>4</sub>)<sub>2</sub> dissolved in sterile PBS (pH = 7.4) and incubated at 37°C for 60 minutes. The treated cells were washed with PBS to remove the remaining metal ions. The culture medium (0.2 mL) was added to the cell culture, which was then treated with a 25  $\mu$ M solution of R1. The samples were incubated at 37°C for 30 minutes. The culture medium was removed, and the treated cells were washed with PBS before observation. Fluorescent images of the cells were obtained using a Leica DMI600 fluorescent microscope. Similar procedures were adopted for the Pb<sup>2+</sup> and Cu<sup>2+</sup> sensing experiments.

### Acknowledgments

SD acknowledges SERB-DST (project no. EMR/2016/002183), and DST-FIST (Project No. SR/FST/CSI-256), Govt. of India for financial assistance. SD was grateful to Prof. Wim Dehaen, KU

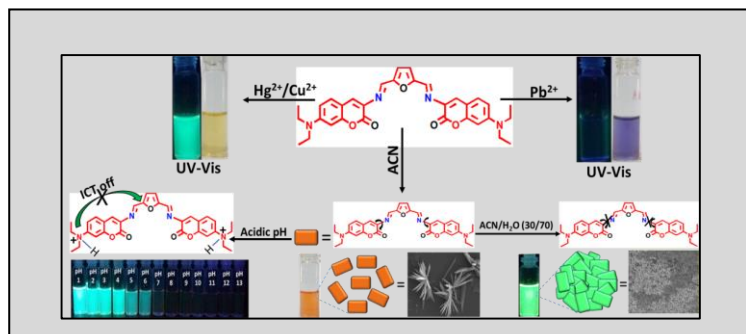
Leuven, Belgium for his valuable suggestion. SKH acknowledges USIC, the University of Burdwan (for Multiskan™ GO facility), DST-SERB, DST-FIST & DST-PURSE programs for research facilities.

**Keywords:** Coumarin-furan • Chemosensor • AIEEE • pH sensor • Pb<sup>2+</sup>, Hg<sup>2+</sup> and Cu<sup>2+</sup>.

- [1] H.-C. Hung, C.-W. Cheng, Y.-Y. Wang, Y.-J. Chen, W.-S. Chung, *Chem. Eur. J.* **2009**, 6360-6366.
- [2] K. Li, J. Cui, Z. Yang, Y. Huo, W. Duan, S. Gong, Z. Liu, *Dalton Trans.* **2018**, 47, 15002-15008.
- [3] H.-H. Kuo, L.-Y. Hsu, J.-Y. Tso, W.-Y. Hung, S.-H. Liu, P.-T. Chou, K.-T. Wong, Z.-L. Zhu, C.-S. Lee, A. K. Y. Jen, Y. Chi, *J. Mater. Chem. C* **2018**, 6, 10486-10496.
- [4] a) S. Samanta, U. Manna, T. Ray, G. Das, *Dalton Trans.* **2015**, 44, 18902-18910; b) M. Suresh, A. Ghosh, A. Das, *Chem. Commun.* **2008**, 3906-3908; c) U. Reddy G, F. Ali, N. Taye, S. Chattopadhyay, A. Das, *Chem. Commun.* **2015**, 51, 3649-3652.
- [5] B. K. Datta, D. Thiyagarajan, A. Ramesh, G. Das, *Dalton Trans.* **2015**, 44, 13093-13099.
- [6] M. Gao, B. Z. Tang, *ACS Sens.* **2017**, 2, 1382-1399.
- [7] a) W. Qin, D. Ding, J. Liu, W. Z. Yuan, Y. Hu, B. Liu, B. Z. Tang, *Adv. Funct. Mater.* **2012**, 22, 771-779; b) F. Ali, H. A. Anila, N. Taye, R. G. Gonnade, S. Chattopadhyay, A. Das, *Chem. Commun.* **2015**, 51, 16932-16935; c) S. Saha, A. Ghosh, P. Mahato, S. Mishra, S. K. Mishra, E. Suresh, S. Das, A. Das, *Org. Lett.* **2010**, 12, 3406-3409; d) S. Saha, M. U. Chhatbar, P. Mahato, L. Praveen, A. K. Siddhanta, A. Das, *Chem. Commun.* **2012**, 48, 1659-1661.
- [8] Y. Xu, L. Ren, D. Dang, Y. Zhi, X. Wang, L. Meng, *Chem. Eur. J.* **2018**, 24, 10383-10389.
- [9] J. Stelzer, C. Vallet, A. Sowa, D. Gonzalez-Abradelo, S. Riebe, C. G. Daniliu, M. Ehlers, C. A. Strassert, S. K. Knauer, J. Voskuhl, *ChemistrySelect* **2018**, 3, 985-991.
- [10] a) M. Suresh, S. Mishra, S. K. Mishra, E. Suresh, A. K. Mandal, A. K. Srivastav, A. Das, *Org. Lett.* **2009**, 11, 2740-2743; b) A. Kumar, D. Sain, C. Kumari, S. Dey, *ChemistrySelect* **2017**, 2, 1106-1110; c) B. A. K. Mandal, M. Suresh, P. Das, E. Suresh, M. Baidya, S. K. Ghosh, A. Das, *Org. Lett.* **2012**, 14, 2980-2983; d) P. Das, A. Ghosh, A. Das, *Inorg. Chem.* **2010**, 49, 6909-6916.
- [11] U. Haldar and H.-I Lee, *Polym. Chem.* **2018**, 9, 4882-4890.
- [12] S. O. Tümay, A. Uslu, H. Ardiç Alidağı, H. H. Kazan, C. Bayraktar, T. Yolaçan, M. Durmuş, S. Yeşilot, *New J. Chem.* **2018**, 42, 14219-14228.
- [13] Z. Mou, Q. Zhuang, H. Xie, Y. Luo, D. Cui, *Dalton Trans.* **2018**, 47, 14985-14991.
- [14] J. Wang, J. Mei, R. Hu, J. Sun, Z. A. Qin, B. Z. Tang, *J. Am. Chem. Soc.* **2012**, 134, 9956-9966.
- [15] Y. Hong, J. W. Y. Lam, B. Z. Tang, *Chem. Soc. Rev.* **2011**, 40, 5361-5388.
- [16] A. Kumar, S. Mondal, K. S. Kashyap, S. K. Hira, P. P. Manna, W. Dehaen, S. Dey, *New J. Chem.* **2018**, 42, 10983-10988
- [17] Y. Hong, J. W. Y. Lam, B. Z. Tang, *Chem. Commun.* **2009**, 0, 4332-4353.
- [18] X. Liu, G. Liang, *Chem. Commun.* **2017**, 53, 1037-1040.
- [19] Y. Yang, C.-Y. Gao, T. Li, *ChemistrySelect* **2016**, 1, 4577-4581.
- [20] J. Chen, C. C. W. Law, J. W. Y. Lam, Y. Dong, S. M. F. Lo, I. D. Williams, D. Zhu, B. Z. Tang, *Chem. Mater.* **2003**, 15, 1535-1546.
- [21] H. Tong, Y. Dong, Y. Hong, M. Häussler, J. W. Y. Lam, H. H. Y. Sung, X. Yu, J. Sun, I. D. Williams, H. S. Kwok, B. Z. Tang, *J. Phys. Chem. C* **2007**, 111, 2287-2294.
- [22] H. Tong, Y. Hong, Y. Dong, Y. Ren, M. Häussler, J. W. Y. Lam, K. S. Wong and B. Z. Tang, *J. Phys. Chem. B*, **2007**, 111, 2000-2007.
- [23] Q. Zeng, Z. Li, Y. Dong, C. A. Di, A. Qin, Y. Hong, L. Ji, Z. Zhu, C. K. W. Jim, G. Yu, Q. Li, Z. Li, Y. Liu, J. Qin, B. Z. Tang, *Chem. Commun.* **2007**, 0, 70-72.
- [24] A. Kumar, C. Kumari, D. Sain, S. K. Hira, P. P. Manna, S. Dey, *ChemistrySelect* **2017**, 2, 2969-2974.
- [25] D. Maity, T. Govindaraju, *Inorg. Chem.* **2011**, 50, 11282-11284.
- [26] D. Maity, T. Govindaraju, *Inorg. Chem.* **2010**, 49, 7229-7231.

- [27] D. Sain, C. Kumari, A. Kumar, H. P. Nayek, S. Dey, *Dalton trans.* **2016**, 45, 9187-9192.
- [28] H. N. Kim, W. X. Ren, J. S. Kim, J. Yoon, *Chem. Soc. Rev.* **2012**, 41, 3210-3244.
- [29] S. Wang, Z. Wang, Y. Yin, J. Luo, L. Kong, *J. Photochem. Photobiol.* **2017**, 333, 213-219.
- [30] A. W. Varnes, R. B. Dodson, E. L. Wehry, *J. Am. Chem. Soc.* **1972**, 94, 946-950.
- [31] J. Wu, W. Liu, J. Ge, H. Zhang, P. Wang, *Chem. Soc. Rev.*, **2011**, 40, 3483-3495
- [32] Q. Li, Y. Li, T. Min, J. Gong, L. Du, D. L. Phillips, J. Liu, J. W. Y. Lam, H. H. Y. Sung, I. D. Williams, R. T. K. Kwok, C. L. Ho, K. Li, J. Wang, B. Z. Tang, *Angew. Chem. Int. Ed.* **2019**, DOI: 10.1002/anie.201909706.
- [33] a) H. Wu, Y. Wang, W.-N. Wu, Z.-Q. Xu, Z.-H. Xu, X.-L. Zhao, Y.-C. Fan *Spectrochim. Acta A* **2019**, 222, 117272; b) C.-r. Li, S.-l Li, Z.-y. Yang *Spectrochim. Acta A* **2017**, 174, 214-222; c) L. He, B. Dong, Y. Liu, W. Lin, *Chem. Soc. Rev.*, **2016**, 45, 6449-6461.
- [34] A. F. Wells, "Structural inorganic chemistry," 5th ed., Clarendon Press, Oxford, **1984**, pp. 1288.
- [35] a) N. Mergu, M. Kim, Y.-A. Son *Spectrochim. Acta A*, **2018**, 188, 571-580; b) S. Mukherjee, S. Hazra, S. Chowdhury, S. Sarkar, K. Chattopadhyay, A. Pramanik *J. Photochem. Photobiol. A* **2018**, 364, 635-644; c) K. Wang, L. Ma, G. Liu, D. Cao, R. Guan, Z. Liu, *Dyes Pigm.*, **2016**, 126, 104-109; d) L. Huang, J. Cheng, K. Xie, P. Xi, F. Hou, Z. Li, G. Xie, Y. Shi, H. Liu, D. Baib, Z. Zeng, *Dalton Trans.*, **2011**, 40(41), 10815-10817.
- [36] a) O. García-Beltrán, A. Rodríguez, A. Trujillo, A. Cañete, P. Aguirre, S. Gallego-Quintero, M. T. Nuñez, M. E. Aliaga, *Tetrahedron Lett.* **2015**, 56, 5761-5766; b) X.-B. Wang, J. Zhou, D. Zhang, B. Wang, *Anal. Methods*, **2016**, 8, 6916-6922; b) S. Wang, Z. Wang, Y. Yin, J. Luo, L. Kong, *J. Photochem. Photobiol. A*, **2017**, 333, 213-219.
- [37] a) D. Wu, W. Huang, C. Duan, Z. Lin Q. Meng, *Inorg. Chem.*, **2007**, 46, 1538; b) S. Goswami, A. Manna, S. Paul, A. K. Maity, P. Saha, C. K. Quah, H.-K. Fun, *RSC Adv.*, **2014**, 4, 34572-34576; c) S. Goswami, S. Paul, A. Manna, *RSC Adv.*, **2013**, 3, 25079-25085.
- [38] P. H. Kumar, V. K. Singh, A. Srivastava, S. K. Hira, P. Kumar, P. P. Manna, *Ceram. Int.* **2015**, 41, 11161-11168.
- [39] S. K. Hira, P. P. Manna, *Cell. Immunol.* **2012**, 275, 69-79.

## Entry for the Table of Contents



The first template-assisted, regio-selective, coumarin-furan conjugated Schiff base chemosensor (**R1**) has been developed for the recognition of  $\text{Pb}^{2+}$ ,  $\text{Hg}^{2+}$ , and  $\text{Cu}^{2+}$  by colorimetric and fluorometric techniques with an intramolecular charge transfer (ICT) *on-off* mechanism. Non-fluorescence **R1** turned into green fluorescent upon addition of  $\text{Hg}^{2+}$  and  $\text{Cu}^{2+}$  and in deep blue with  $\text{Pb}^{2+}$ . **R1** functioned as a pH sensor and showed excellent AIEE, observed through the naked eye. The needle-shaped sensor exhibited maximum aggregation when the size was increased by 70 fold (2.2 to 157.4 nm) measured in DLS.